Astron. Astrophys. 323, 235–242 (1997)

ASTRONOMY AND ASTROPHYSICS

Solar P-mode frequencies from the IRIS network

B. Gelly[1], D. Fierry-Fraillon[1], E. Fossat[1], P. Palle[2], A. Cacciani[3], S. Ehgamberdiev[4], G. Grec[5], J.T. Hoeksema[6], S. Khalikov[4], M. Lazrek[5,7], S. Loudagh[1], A. Pantel[1], C. Regulo[2], and F.X. Schmider[1]

[1] Département d'Astrophysique, URA CNRS 709, Université des Sciences, F-06108 Nice Cedex 2, France
[2] Instituto de Astrofísica de Canarias, E-38071 La Laguna, Tenerife, Spain
[3] Dipartimento di Fisica dell'Università, Piazzale Aldo Moro 2, I-00185 Roma, Italia
[4] Astronomical Institute of the Uzbek Academy of Sciences, Astronomicheskaya 33, Tashkent-700052, Uzbekistan
[5] Département Cassini, URA CNRS 1362, Observatoire de la Côte d'Azur, B.P. 229, F-06304 Nice Cedex 4, France
[6] Center for Space Science and Astrophysics, Stanford University, Stanford, CA 94305, USA
[7] Laboratoire d'Astronomie du CNCPRST, BP 1346, Rabat, Morocco

Received 24 September 1996 / Accepted 23 December 1996

Abstract. The Iris network for helioseismology has operated since 1989. We present tables of solar p-mode frequencies for observations taken during the four summer seasons from 1989 to 1992. This analysis uses the technique of maximum likelihood fitting and a χ^2_2 model for the probability density function of the spectrum. The simultaneous fitting of odd and even pairs of peaks strengthens the identification of the $\ell = 3$ eigenmodes and improves the error bars on the $0-2$ group. The frequencies are in good agreement with other observational results and with theoretical values for the D_0 and the $\Delta\nu$ parameters of the asymptotic approximation. A decrease of $0.25 \pm 0.12\ \mu Hz$ is seen between the 1989 and the 1992 data sets. The change is associated with the decrease of solar activity and is comparable with results of previous studies.

Key words: Sun: oscillations; activity

1. Introduction

Precise measurement of solar p-mode frequencies is one of the main goals of helioseismology observations. Since the first individual p modes were identified in the power spectra of full disk observations (Grec et al. 1980; Claverie et al. 1981), tables of frequencies have been essential for testing solar models. At the time, inversions using those frequencies were able to address the problem of the helium content of the Sun and place bounds on the heavy element abundance. The results indicated that the Sun was in fact quite close to the standard model, but with a deeper convection zone than was generally expected. Although surprisingly good (a few percent departure), the results of those first inversions could not be easily compared with the standard solar model due to the lack of precision in the theoretical frequencies compared to the observations. Recent advances in the study of solar structure have come from the understanding of these uncertainties and of their effects on the inversions (Christensen-Dalsgaard 1990), refinements in the atomic physics leading to a better equation of state for the solar interior (Däppen et al. 1991; Christensen-Dalsgaard et al. 1992), and the use of p-mode frequencies spanning the low and intermediate ℓ-range observed by a single instrument (LOWL) (Basu et al. 1996).

From the data analysis point of view, improvements in the frequency determinations have come from more sophisticated models of the spectral peaks (Jimenez et al. 1994, Elsworth et al. 1994) and from improved understanding of the first order statistics of the power spectra of the eigenmodes. The present work builds on these latter ideas.

Send offprint requests to: gelly@irisalfa.unice.fr

2. IRIS full disk data and analysis

The IRIS network for full disk helioseismology (Fossat 1991) has been operated as a multisite network since 1989, and was completed in 1994 with the installation of the Australian site at Narrabri. In this paper we analyze the merged data from 1989 to 1992.

The first two instruments of the network were installed in 1988 on the mountaintop sites of Kumbel in Uzbekistan and Oukaimden in Morocco; they began providing useful data in 1989. In the same year a third site came into operation at Izaña, Tenerife. Prototype instruments at La Silla, Chile and Stanford, California were upgraded and began taking good quality measurements in 1990 and 1991. Later on, the network was completed by adding the Culgoora, Australia site and augmented by agreements signed with the BiSON network and with A. Cacciani. It is presently possible to combine the IRIS sodium cell data with that of the magneto-optical filter (MOF) instrument

Table 1. The sites are: K: Kumbel, Uzbekistan; O: Oukaimden, Morocco; T: Teide, Tenerife, Spain; M: Mark-1, Tenerife, Spain; E: European Southern Observatory, La Silla, Chile; W: Wilcox Solar Observatory, Stanford, CA, U.S.A.; J: Jet Propulsion Laboratory, Pasadena, CA, U.S.A.)

Years	1989	1990	1991	1992
Iris sites	K,O,M,T,J	K,T	K,O,T,E	K,T,W
Start Date	Jul04	Jun05	Jul01	Jun14
End Date	Nov14	Oct11	Oct23	Oct28
Hours	1343.9	1463.9	1580.5	1702.6
Duty cycle(%)	41.9	47.5	57.3	52.2

(Cacciani et al. 1988) operated at JPL during several summers since 1989, and also the data of the BiSON network Mark-1 potassium cell instrument in Tenerife (Elsworth et al. 1988) since the same year.

The data analyzed in this paper resembles that of a partially deployed network. Several instruments encountered more or less extended down times due to various problems, from thunderstorms to optical and technical difficulties of many kinds that any instrumentalist can easily imagine. To get the best combination of temporal coverage and data quality we have selected four northern summer intervals with duty cycles from 40% to 60%.

Table 1 summarizes the data analyzed in this paper. Raw data from the various sites are first timed and calibrated using the known Earth rotation in a process described by Palle et al. (1993). The calibrated data points are resampled on an even U.T. grid and can then be merged in various ways depending on the analysis to be done. We have used the weighted merging described by Fossat (1992). Fig. 1 shows the power spectrum of the merged dataset for 1991.

The effect of the temporal window, which is still present in the power spectrum of Fig. 1, has been efficiently reduced using a Richardson-Lucy deconvolution algorithm (Pantel 1996) applied to either the direct (0-1) window function or to the weighted window function. This provides an improved signal to noise performance in the lower frequency range. The increase in SNR at low frequency leads to a more accurate identification of modes in a larger frequency range, where $n \leq 13$. The cleaning of the daily sidelobes minimizes the contamination of the peaks by sidelobes of other peaks when determining the frequencies, which is otherwise a major concern.

3. Peak parameter extraction techniques

The simple model of a solar eigenmode as a damped one-dimensional oscillator has been very widely used in the recent years. This model allows one to assume that the peaks in the natural Fourier spectrum of Fig. 1 are asymptotically described by Lorentz profiles, namely:

$$L_{n,\ell}(\nu) = \frac{A}{1 + \left(\frac{\nu - \nu_{n,\ell}}{\Gamma}\right)^2} + B \qquad (1)$$

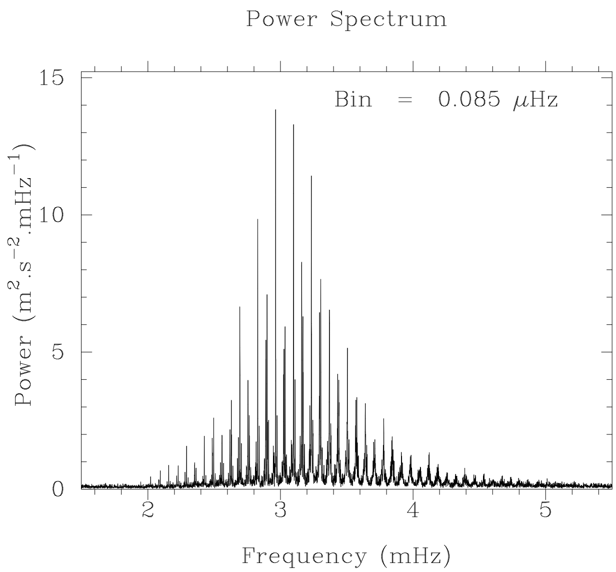

Fig. 1. The 1991 power spectrum. At the scale shown here the daily sidelobes coming from having "only" a 57% duty cycle are not visible. The first sidelobes still contain 25% of the power of the central peak.

where A is the amplitude of a peak of width 2Γ at a frequency $\nu_{n,\ell}$, having a background noise B.

- This assumption is strictly true only for the $\ell = 0$ modes. It may be true for the individual components of any split mode, but only if the splitting is visible and if each component can be measured separately. This is not, however, generally the case.
- The assumption is less appropriate for $\ell > 0$ modes when the splitting is unresolved. In this case the interference between the visibly split components and the interference between each component and the noise (depending on the SNR of the portion considered) create a very complex situation that leads to a greater uncertainty in the determination of the central frequency. Moreover the FWHM that would be determined for such peaks using a single Lorentz profile would actually be a combination of the actual width of the mode and of the splitting of the components.

To address this problem we prefer to model the power spectrum as a suitable combination of many such profiles.

3.1. Power spectrum modeling

The succession of pictures in Fig. 2 illustrates the increasing difficulty of separating individual $\ell = 0$ and $\ell = 2$ modes with increasing frequency. The difficulty has three main causes:

- in this frequency range, the separation between $\ell = 0$ and $\ell = 2$ is comparable to the distance from the central peak to its first sidelobe; the first higher frequency sidelobe of $\ell = 2$ actually lies inside the nearest $\ell = 0$ peak and *viceversa*.
- the mode lifetimes are shorter at higher frequencies, therefore they tend to blend into each other because of the broadening of the profile.

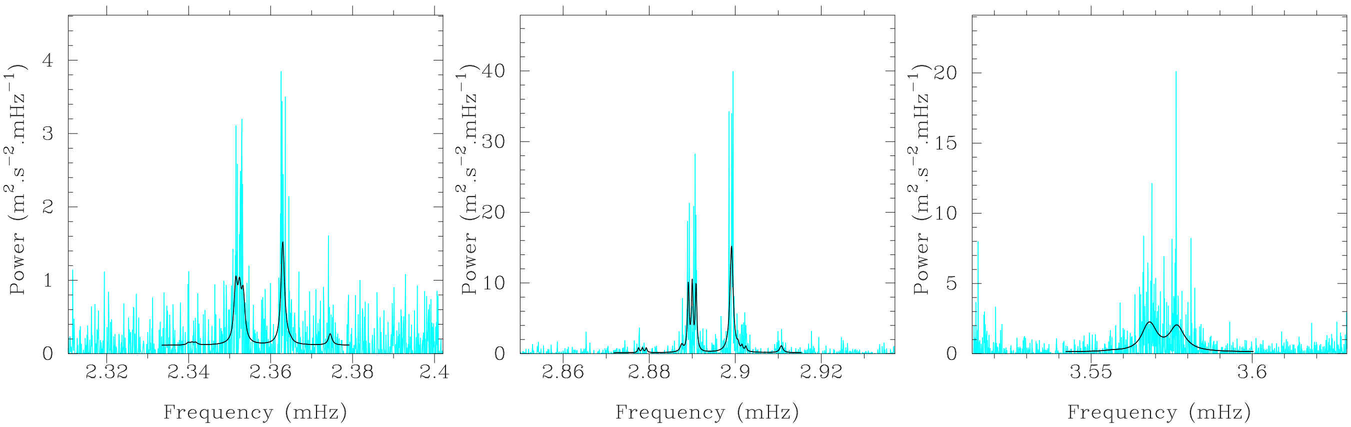

Fig. 2. Power spectra of $\ell = 2$ and $\ell = 0$ modes for $n = 16, 20, 25$ (left to right). The $\ell = 0$ peak is on the right in each panel. Note the increasing difficulty of identifying the two components due to their blending and to the decrease in the SNR (note the difference in the scales). The superimposed curve is a 9 parameter fit that models the profiles of the two modes and their sidelobes. $\ell = 2$ is taken to be a triplet with 3 identical amplitudes. A simpler model was used at frequencies higher than 3.6 mHz to improve the identification of the 2 modes.

- the SNR is decreasing.

In a similar way, Fig. 3 illustrates the increasing difficulty of separating $\ell = 1$ and $\ell = 3$ peaks. Here the problem is simpler, in one sense, because the separation is not equal to the sidelobe separation, but in another sense it is more complicated because of the lower amplitude of the $\ell = 3$ modes. The amplitude is less because of the reduced sensitivity of the full disk observations to $\ell = 3$ modes.

We parameterize the $\ell = 0$ and $\ell = 2$ groups by modeling the $\ell = 0$ peak as a single Lorentz profile plus sidelobes, and the $\ell = 2$ peaks as a triplet, where each component of the triplet has its own pair of sidelobes. The fits were determined simultaneously in the frequency range containing each even group. The same procedure was performed for the odd groups, $\ell = 1$ being a doublet with sidelobes and $\ell = 3$ being a quadruplet mode. However, we neglected the quadruplet sidelobes, assuming they were too weak to interfere.

We decided to impose a single model "splitting" value for all modes. This "splitting" was fixed at a sidereal value of 466 nHz and all the frequencies were computed. Our team recently published a lower value of 451 nHz, determined using a weighted average over several ℓ and n (Lazrek et al., 1996), but one should keep in mind that the low-l averaged splitting values found in the litterature range from 414 nHz (Chaplin et al. 1996) to 510 nHz (Jimenez et al. 1994). Accordingly, we verified that a change of the splitting value in the range from 400 to 500 nHz affects the central frequencies of about $25 - 75$ nHz, an amount much less than our 1σ error bars which are typically of $150 - 200$ nHz. Of course our future work will use the actual low-ℓ mode splittings computed from the latest data sets, including those of the space instruments onboard SOHO: GOLF, VIRGO, LOI and MDI.

Above 3.6 mHz ($n = 26$), our SNR no longer allows identification of $\ell = 3$ and we only determine the $\ell = 1$ frequencies. For the $0 - 2$ group we abandon the triplet profile for the $\ell = 2$. Nevertheless, it remains possible to fit 2 single Lorentz profiles with a free separation up to about 4.2 mHz, even though the naked eye would not distinguish the $\ell = 0$ from the $\ell = 2$ in some of the data sets. Those modes are labeled in the tables as 'prospective fittings'. When the fit fails but there is still some energy above the noise in the power spectrum, we have fit a single Lorentz profile and labeled the frequency as the average of the $\ell = 0 - 2$ group.

This technique produced most of the entries in Tables 3, 4, 5, and 6.

Below 2 mHz modes may or may not be visible, depending on the SNR of the dataset. We carefully explored this part of the spectrum using the Richardson-Lucy deconvolution spectrum to minimize the sidelobes, as well as maximum entropy spectral estimation to enhance the visibility of the faint peaks; we also averaged spectra across the years. The result of this analysis produced the low-n frequencies in Table 2.

3.2. Fitting technique

Following several authors who have attempted to estimate or actually determine the probability density function (PDF) of a Fourier spectrum (Woodard 1984; Andersen et al.1990; Toutain et al. 1994; Lazrek 1993), we have used a χ^2_2 distribution in a maximum likelihood fitting procedure. As shown by Gabriel (1993), this estimate is only valid in the case of statistically independent points in a Fourier spectrum. Even though our points are not independent, since we use 2^n FFT algorithms with zero padding when no data are available, the PDF of a 50% duty cycle Fourier spectrum is still a χ^2_2 distribution, but with a different slope in log scale. After deconvolution, the independence of the spectral bins is much better and Pantel (1996) has verified that χ^2_2 distributions are a correct approximation of the true PDF.

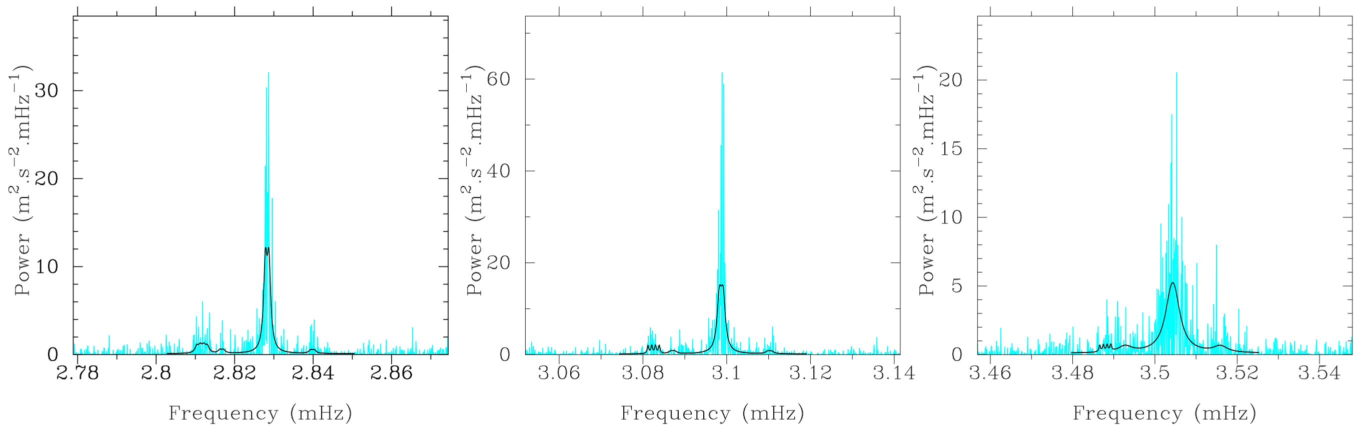

Fig. 3. The panels show $\ell = 1$ and $\ell = 3$ modes for $n = 19, 21, 24$ (left to right). The problem here is distinguishing the left sidelobe of $\ell = 1$ from the quadruplet mode $\ell = 3$. The superimposed curve is from a model which assumes that $\ell = 1$ is a doublet (and therefore has doublet sidelobes) and that $\ell = 3$ has 4 components. At higher frequencies we just give the central frequency of the energy envelope.

Table 2. Low frequency p modes determined from all 4 years analysed in this paper. The error bars are taking into account the number of detection of the peaks (1, 2 or 3 times), the SNR, and the spectral bin. 1: poor SNR. 2: the frequency is slightly varying from one year to the next. 3: SNR is poor and the identification subject to caution. If it is well identified, the error bar should be small. 4: Mostly one year (1992). 5: Problematic error, this mode is already variable

Order	l=0	l=1	l=2	l=3
10	1548.25 ± 0.05	1612.72 ± 0.10^{3}	1674.20 ± 0.15^{4}	
11	1686.63 ± 0.06	1749.32 ± 0.06	1810.28 ± 0.10	
12	1822.25 ± 0.10^{1}	1885.35 ± 0.15	1945.98 ± 0.10	2002.41 ± 0.83
13	1957.50 ± 0.10^{2}	2020.66 ± 0.21^{5}	2082.41 ± 0.44	2138.39 ± 0.60

Table 3. P-mode frequencies derived from the 1989 dataset. 1: 'Prospective fitting', as described in the text. In this case the error bars are underestimated. 2: Average frequency of the 0-2 group.

Order	l=0	l=1	l=2	l=3
12			1946.33 ± 0.51	2002.45 ± 0.14
13	1956.90 ± 0.31	2020.91 ± 0.10	2082.51 ± 0.29	2139.95 ± 1.12
14	2093.25 ± 0.19	2156.56 ± 0.25	2217.33 ± 0.57	
15	2228.42 ± 0.21	2291.99 ± 0.25	2352.75 ± 0.31	2407.85 ± 0.20
16	2362.71 ± 0.22	2425.88 ± 0.14	2485.54 ± 0.29	2542.65 ± 0.37
17	2496.66 ± 0.24	2559.31 ± 0.20	2619.63 ± 0.27	2676.06 ± 0.37
18	2629.97 ± 0.21	2693.54 ± 0.32	2754.93 ± 0.30	2811.75 ± 0.28
19	2764.48 ± 0.18	2828.27 ± 0.24	2889.47 ± 0.36	2947.63 ± 0.47
20	2899.24 ± 0.26	2963.51 ± 0.15	3024.66 ± 0.25	3083.14 ± 0.43
21	3034.38 ± 0.29	3098.61 ± 0.15	3160.24 ± 0.45	3217.95 ± 0.37
22	3168.83 ± 0.29	3233.47 ± 0.29	3295.51 ± 0.78	3353.71 ± 0.40
23	3304.46 ± 0.36	3369.31 ± 0.37	3430.70 ± 0.90	
24	3439.67 ± 0.52	3504.53 ± 0.35	3567.42 ± 0.62	
25	3576.07 ± 0.77	3640.41 ± 0.48	3701.66 ± 0.60^{1}	
26	3711.42 ± 0.70^{1}	3775.44 ± 0.37	3838.86 ± 0.56^{1}	
27	3846.16 ± 0.62^{1}	3912.53 ± 0.69	3975.38 ± 0.75^{1}	
28	3984.66 ± 0.80^{1}	4048.29 ± 0.62	4112.64 ± 0.87^{1}	
29	4124.01 ± 0.93^{1}	4186.24 ± 0.83		
30	4259.39 ± 0.98^{2}	4323.07 ± 0.93		
31		4460.74 ± 0.62		

Table 4. P-mode frequencies derived from the 1990 dataset. 1: 'Prospective fitting', as described in the text. In this case the error bars are underestimated. 2: Average frequency of the 0-2 group.

Order	l=0	l=1	l=2	l=3
12				2001.36 ± 0.25
13		2020.11 ± 0.23	2082.33 ± 0.13	2137.75 ± 0.10
14	2093.76 ± 0.09	2156.83 ± 0.09	2217.61 ± 0.22	2274.13 ± 0.17
15	2228.87 ± 0.14	2291.91 ± 0.11	2352.32 ± 0.18	2407.37 ± 0.20
16	2362.93 ± 0.17	2425.40 ± 0.12	2485.70 ± 0.25	2542.19 ± 0.17
17	2496.30 ± 0.18	2559.49 ± 0.11	2619.82 ± 0.16	2676.39 ± 0.21
18	2629.37 ± 0.13	2693.53 ± 0.14	2754.56 ± 0.16	2811.67 ± 0.28
19	2764.65 ± 0.15	2828.25 ± 0.15	2889.44 ± 0.22	2947.60 ± 0.38
20	2899.11 ± 0.18	2963.65 ± 0.15	3024.53 ± 0.40	3082.83 ± 0.35
21	3034.38 ± 0.21	3098.59 ± 0.14	3159.72 ± 0.18	3218.75 ± 0.33
22	3169.25 ± 0.15	3233.52 ± 0.17	3295.41 ± 0.25	3354.17 ± 0.44
23	3304.12 ± 0.19	3368.60 ± 0.21	3430.27 ± 0.29	3490.79 ± 0.45
24	3438.83 ± 0.22	3504.56 ± 0.20	3567.76 ± 0.31	
25	3574.88 ± 0.31	3640.53 ± 0.29	3702.94 ± 0.76^{1}	
26	3712.23 ± 0.65^{1}	3775.95 ± 0.53	3841.00 ± 0.84^{1}	
27	3849.06 ± 0.94^{1}	3911.49 ± 0.62	3978.19 ± 0.93^{1}	
28	3986.31 ± 1.11^{1}	4051.29 ± 0.66	4112.11 ± 1.47^{1}	
29	4120.50 ± 1.30^{1}	4187.13 ± 0.71	4252.97 ± 1.69^{1}	
30	4259.43 ± 1.33^{1}	4322.75 ± 0.94		
31	4393.11 ± 1.15^{2}	4463.13 ± 1.16		

Table 5. P-mode frequencies derived from the 1991 dataset. 1: 'Prospective fitting', as described in the text. In this case the error bars are underestimated. 2: Average frequency of the 0-2 group. 3: Only visible on the MEM spectrum.

Order	l=0	l=1	l=2	l=3
11			1811.07 ± 0.16^{3}	
12		1884.87 ± 0.14^{3}	1946.26 ± 0.08	2002.71 ± 0.10
13	1956.43 ± 0.15	2020.93 ± 0.07	2082.48 ± 0.19	2140.05 ± 0.15
14	2093.60 ± 0.13	2156.92 ± 0.07	2217.80 ± 0.99	2274.17 ± 0.12
15	2228.76 ± 0.32	2292.15 ± 0.08	2352.41 ± 0.22	2407.71 ± 0.41
16	2362.98 ± 0.18	2425.47 ± 0.14	2486.33 ± 0.06	2542.32 ± 0.33
17	2496.46 ± 0.08	2559.21 ± 0.13	2620.23 ± 0.19	2676.03 ± 0.34
18	2629.81 ± 0.15	2693.64 ± 0.13	2754.66 ± 0.14	2811.71 ± 0.22
19	2764.60 ± 0.15	2828.30 ± 0.13	2890.00 ± 0.08	2947.33 ± 0.28
20	2899.14 ± 0.08	2963.73 ± 0.14	3024.95 ± 0.21	3082.55 ± 0.26
21	3034.38 ± 0.18	3098.71 ± 0.15	3160.57 ± 0.12	3217.85 ± 0.39
22	3169.06 ± 0.11	3233.35 ± 0.17	3295.40 ± 0.27	3353.97 ± 0.90
23	3303.95 ± 0.18	3368.64 ± 0.26	3431.10 ± 0.37	3487.86 ± 0.61
24	3440.09 ± 0.31	3504.39 ± 0.31	3568.08 ± 0.56	
25	3576.91 ± 0.53	3640.31 ± 0.26	3702.80 ± 1.16	
26	3712.07 ± 0.30	3777.79 ± 0.30	3840.35 ± 1.15^{1}	
27	3846.27 ± 1.27^{1}	3911.92 ± 0.70	3975.58 ± 1.02^{1}	
28	3985.20 ± 1.03^{1}	4050.57 ± 0.77	4113.59 ± 1.14^{1}	
29	4122.27 ± 1.24^{1}	4186.73 ± 0.71		
30	4256.33 ± 0.81^{2}	4323.44 ± 0.91		
31	4394.10 ± 1.15^{2}	4461.72 ± 1.07		
32	4532.31 ± 1.95^{2}			

Table 6. P-mode frequencies from the 1992 dataset. 1: 'Prospective fitting', as described in the text. In this case the error bars are underestimated. 2: Average frequency of the 0-2 group.

Order	l=0	l=1	l=2	l=3
12				2002.87 ± 0.12
13		2020.77 ± 0.06	2082.40 ± 0.27	2138.78 ± 0.15
14	2093.91 ± 0.26	2157.19 ± 0.10	2217.61 ± 0.16	2274.46 ± 0.06
15	2228.78 ± 0.14	2292.15 ± 0.04	2351.85 ± 0.26	2407.53 ± 0.12
16	2362.82 ± 0.17	2425.58 ± 0.08	2485.57 ± 0.21	2541.77 ± 0.13
17	2496.59 ± 0.20	2559.06 ± 0.09	2619.02 ± 0.38	2676.10 ± 0.21
18	2629.56 ± 0.20	2693.23 ± 0.16	2754.63 ± 0.13	2811.54 ± 0.21
19	2764.09 ± 0.10	2828.20 ± 0.11	2889.86 ± 0.14	2947.69 ± 0.37
20	2899.12 ± 0.11	2963.28 ± 0.16	3025.36 ± 0.11	3082.04 ± 0.34
21	3033.95 ± 0.09	3098.33 ± 0.14	3160.00 ± 0.21	3218.85 ± 0.51
22	3168.83 ± 0.20	3233.29 ± 0.15	3294.81 ± 0.22	3353.24 ± 0.59
23	3304.12 ± 0.20	3368.88 ± 0.16	3430.78 ± 0.26	3489.37 ± 0.37
24	3440.09 ± 0.27	3504.31 ± 0.21	3567.19 ± 0.67	
25	3575.40 ± 0.39	3640.19 ± 0.31	3703.88 ± 0.44[1]	
26	3712.58 ± 0.36[1]	3776.55 ± 0.30	3841.74 ± 0.88[1]	
27	3847.42 ± 0.91[1]	3912.12 ± 0.42	3983.57 ± 0.70[1]	
28	3976.93 ± 0.67[1]	4049.82 ± 0.48		
29	4117.53 ± 0.59[2]	4186.46 ± 0.41		
30		4321.23 ± 0.72		

3.3. Error bars in frequency

The first estimation of our error bars is based on Duvall's formula (Duvall 1990) for a singlet mode:

$$\sigma = \sqrt{\frac{\Gamma}{4\pi T d}} \tag{2}$$

This formula takes into account the normalized duty cycle d, the duration of the observation T and the speckle pattern produced by random excitation. But to account for the signal-to-noise ratio, it is necessary to go through all the actual computations using the assumptions of the previous section (Lorentz profile, χ^2_2distribution, and minimization). The solution becomes (Libbrecht 1992, Toutain et al. 1994):

$$\sigma_{th} = \sqrt{\frac{\Gamma}{4\pi T d}} f(\beta) \tag{3}$$

where $f(\beta)$ is a function of B/A, the ratio of the noise, B, over the mode amplitude, A, as defined in Eq. 1. This dimensionless function ranges from 1 if there is no noise to about 20 if the noise is comparable to the signal. Still, this formula does not account for:

- the interference between a peak and the sidelobes of its immediate neighbors
- the determination of the split components
- the interference among the split components

So, we have used a Monte Carlo (MC) approach to address this question. The technique can be described as a 3 stage process:

- in a given frequency range we perform a maximum likelihood fit in order to extract a set of initial peak parameters.
- using these initial values we generate many instances of the spectrum using random perturbations. A fit is performed on each simulation to determine the noisy parameters.
- from this we can model the probability density function of each parameter and evaluate its statistical uncertainty.

For determining frequency, about 150 realizations are necessary to ensure the convergence of the MC mean toward the initial parameter and we used 400 iterations in the computations of the PDF. The PDF is symmetric around the mean value (Fig. 4), suggesting that it can be modeled by a Gaussian distribution:

$$f(\nu) = A \ \exp \frac{(\nu - m_\nu)^2}{2\sigma_\nu^2} \tag{4}$$

where σ_ν defines the error-bar for each frequency as a statistical uncertainty and is the value quoted in our tables.

4. Comparisons and results

4.1. D_0-$\Delta\nu$ diagram

Rather than compare the individual frequencies of several data sets, we have chosen to compare the classical helioseismic parameters D_0 and $\Delta\nu$ from the asymptotic approximation of frequencies. These two parameters are easy to derive from the frequency datasets and have widely accepted definitions. We have compared the four sets of frequencies from the IRIS network with the BiSON network p-mode frequencies (Elsworth et al. 1994), with the LOWL frequencies (Tomczyk et al. 1996), with two sets of theoretical frequencies computed by the Nice Observatory team (Morel et al. 1996), and another set computed by the Saclay group (Turck-Chièze et al. 1993).

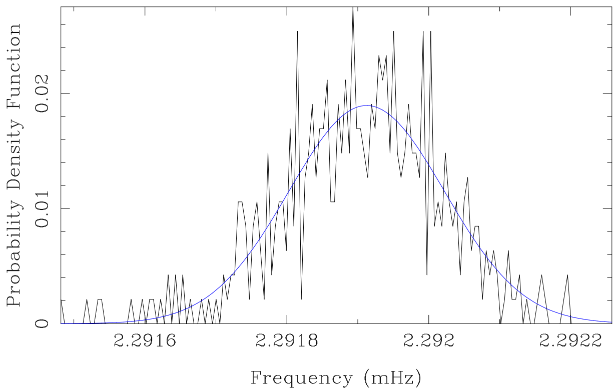

Fig. 4. The probability density function of the n = 15, ℓ = 1 mode for the 1990 dataset in the MC simulation. The superimposed Gaussian fit gives m_ν = 2291.91μHz and σ_ν = 0.11μHz.

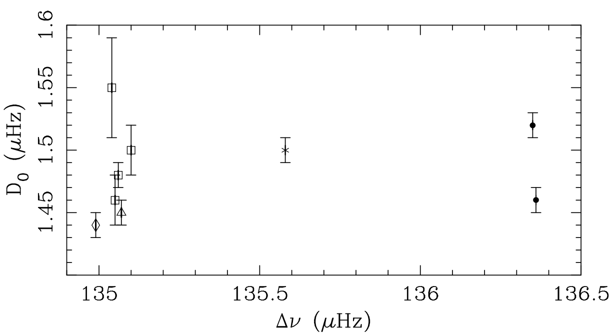

Fig. 5. $D_0 - \Delta_\nu$ plot using 4 IRIS frequency tables (□), Bison frequency table (◇), LOWL frequency table (△), P. Morel et al. theoretical frequency tables (•) for models with and without diffusion, and S. Turck-Chièze et al. theoretical frequency table ($*$) for a model without diffusion.

We derived the "big separation," $\Delta\nu$, using a second order polynomial fit of the echelle-diagram of the datasets from n = 14 to n = 25, and the D_0 parameter from a first order fit to the $\nu_{n,0} - \nu_{n-1,2}$ ("small separation") quantity as previously described (Scherrer et al. 1983; Christensen-Dalsgaard 1988; Gelly et al. 1988), taking n_0 = 22.

Fig. 5 summarizes our results. As a general comment, all observations are consistent with the same value of D_0 and are also compatible with all the models. For $\Delta\nu$ the errors bars are so small that they are not visible at the scale of the figure. Clearly all the observations lie on the left side of the figure and all the theoretical values on the right side. Simply using the meaning of $\Delta\nu$ in the asymptotic approximation, we interpret this discrepancy to some weakness in the treatment of the surface layers of the solar models. Comparisons of other seismological parameters derived from the same frequency tables lead to the same conclusion (Pantel 1996).

4.2. Solar cycle effects

The three years 1989-91 correspond to the maximum phase of solar activity, with a peak in the summer of 1989. In 1992 (last year of our study) solar activity underwent a precipitous fall toward its minimum. We have evaluated the frequency decrease due to solar cycle effects from 1989 to 1992 by computing the average frequency difference over a selected range of n: $< \delta\nu_\ell >_n = < \nu_{n,\ell}(1989) - \nu_{n,\ell}(1992) >_n$. Fig. 6 shows that the mean shift was 0.25 ± 0.12 μHz for ℓ = 0 and ℓ = 1 p modes for n in the range $17 - 24$. This is in good agreement with the BiSON result (Elsworth et al. 1994).

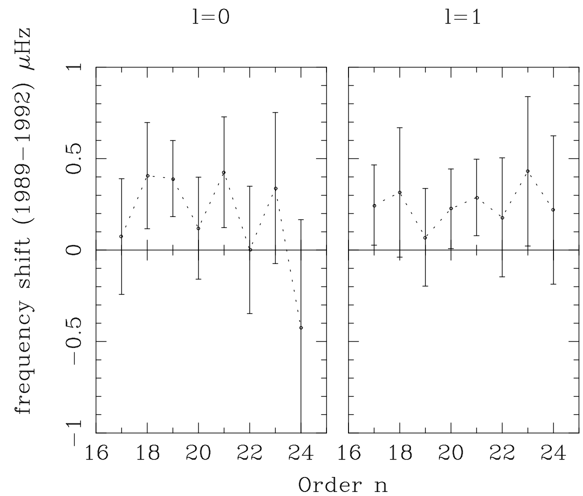

Fig. 6. P-mode frequency shift from 1989 to 1992 showing the same mean shift of 0.25 ± 0.12 μHz for all ℓ = 0 and ℓ = 1 modes, except n = 24, ℓ = 0.

The frequency dependence of the shift seen by other authors (Libbrecht et al. 1990) and the possible ℓ dependence (Palle et al. 1989, Anguera Gubau et al. 1991) are not discernable here because of the limited number of modes and the small number of power spectra. Such a study would require more data, but the quality of the individual frequencies measurement already allows a good determination of the mean frequency shift during this 3-year interval.

5. Conclusions

We are confident that the fitting strategy described in Sect 3.1 gives an unbiased determination of the frequencies below 4 mHz. From the frequency tables presented here we determine values of D_0 and $\Delta\nu$ that are in good agreement with our previous work and with other sets of observational frequencies. By direct subtraction of mode frequencies found in 1989 and 1992, we find a decrease in mode frequencies of 0.25 ± 0.12 μHz. The error bars, computed using a Monte Carlo method, are somewhat higher than previous published values (Elsworth et al., 1994). This is not only due to IRIS network's lower 50% duty cycle, but also because the Monte Carlo method more completely accounts for additional uncertainties in the identification of the p-mode frequencies. Such errors are underrated by the classical formulas. For data sets with higher duty cycles (above 85 %) the Monte-Carlo estimations of the error bars converge toward the values given by the theoritical formulas.

We have analyzed four summer seasons of IRIS network data. Eight years of data already exist, so we shall soon be able to obtain a much more complete list of full disk frequencies that sample the solar cycle from maximum to minimum. Although the now fully-deployed IRIS network has not been able to get as close to the ideal 100% duty cycle as originally intended, many collaborations have been developed, and it is presently possible to merge full disk data not only from the IRIS instruments, but also from Cacciani's MOF, from the BiSON Mark-1 at Tenerife, from GONG integrated images, and possibly from the LOWL integrated images, so that we expect to be close to 100% starting in 1995. This will improve the statistics, reduce the uncertainty levels, and allow us to extend the current limits of p-mode detectability at both low and high frequencies. Of course the extremes of the spectrum will be better investigated using the data from the helioseismology experiments on the SOHO spacecraft, which began operation in 1996. The GOLF experiment, in particular, is most like the IRIS instruments and has proved to be much less noisy at low frequency and has the advantages of total continuity and homogeneous data quality at all frequencies.

Acknowledgements. Data from the IRIS network depends on the coordinated efforts of many peoples from several nations. The authors wish to thank those who have conceived the instrument: E. Fossat and G. Grec; those who have contributed to build and maintain all instruments on site: B. Gelly, J.F. Manigault, G. Rouget, J. Demarcq, G. Galou, A. Escobar, J.M. Robillot; those who have operated the observing sites: M. Baijumamov, S. Ehgamberdiev, S. Ilyasov, S. Khalikov, I. Khamitov, G. Menshikov, S. Raubaev, J.T. Hoeksema, Z. Benkhaldoun, M. Lazrek, S. Kadiri, H. Touma, M. Anguera, A. Jimenez, P.L. Palle, A. Pimienta, C. Regulo, T. Roca Cortes, L. Sanchez, F.X. Schmider; R. Luckhurst, those who have developed the analysis software: S. Ehgamberdiev, S. Khalikov, E. Fossat, B. Gelly, M. Lazrek, P.L. Palle, L. Sanchez, E. Gavryuseva, V. Gavryusev; and those who have contributed to the success of the IRIS project in other critical ways: P. Delache, D. Gough, I. Roxburgh, F. Hill, T. Roca-Cortes, G. Zatsepin, T. Yuldashbaev, L. Woltjer, H. Van der Laan, D. Hofstadt, J. Kennewell, D. Cole, P. Scherrer, F. Sanchez, J.P. Veziant and the Birmingham University Solar Network for sharing the observational facility in Tenerife.
We wish to thank Steve Tomczyk and Jesper Schou in making available to us the LOWL frequency tables.
The IRIS network was funded and is supported by the Institut National des Sciences de l'Univers (INSU) and the Centre National de la Recherche Scientifique (CNRS).

References

Andersen E.R., Duvall Jr T.L., Jefferies S.M., 1990, ApJ 364, 699
Anguera Gubau M., Palle P.L., Perez Hernandez F., Regulo C., Roca Cortes T., 1991, A&A 255
Basu S., Christensen-Dalsgaard J., Schou J., Thompson M.J., Tomczyk S., 1996, Bull. Astron. Soc. India, 24, in press
Cacciani A., Rosati P., Ricci D., Marquedant R., Smith E., 1988, in Seismology of the Sun and Sun-Like Stars, ed. E.J. Rolfe, Paris: ESA SP-286, 181-184
Chaplin W.J., Elsworth Y., Howe R. et al., 1996, MNRAS 280, 49-53
Claverie A., Isaak G. R., Mcleod C. P., Van Der Raay H. B., Roca Cortes T., 1981, Nature 293, 443
Christensen-Dalsgaard J., 1988, Proc. IAU Symposium 123, Christensen-Dalsgaard J. & Frandsen S. Eds., Reidel, Dordrecht, 295-298
Christensen-Dalsgaard J., 1990, in Challenges to Theories of the Structure of Moderate Mass Stars, Lecture Notes in Physics, eds. Gough D.O. & Tomree J., Springer, Heidelberg
Christensen-Dalsgaard J. , Däppen W., 1992, A&AR vol.4, no. 3, 267
Däppen W., Keady J., Rogers, Forrest, 1991, Solar interior and atmosphere (A92-36201 14-92). Tucson, University of Arizona Press, 112-139
Duvall Jr.T.L., 1990, in I.A.U. Colloq. 121 Inside the Sun, Berthomieux & Cribier M. eds., (Dordretch Kluwer), 253
Elsworth Y.P., Isaak G.R., Jefferies S.M., McLeod C.P., New R., van der Raay H.B., Palle P.L., Regulo C., Roca Cortes T., 1988, in Advances in Helio- and Asteroseismology, IAU Symp. 123, ed. J. Christensen-Dalsgaard, and S. Frandsen, Dordrecht: Reidel, 535-539
Elsworth Y., Howe R., Isaak G.R. et al., 1994, ApJ 434, 801
Fossat E., 1991, Solar Physics, 133, 1-12
Gabriel M., priv. comm. , 1993
Gelly B., Fossat E., Grec G., Schmider F.X., 1988, A&A 200
Grec G., Fossat E., and Pomerantz M.A. 1980, Nature 288, 541
Jimenez A., Perez Hernandez F., Claret A., Palle P.L., Regulo C., Roca Cortes T., 1994, ApJ 435, 874
Lazrek M., 1993, Thesis, Université de Liège
Lazrek M., Pantel A., Fossat E. et al., 1996, Solar Physics, 166, 1
Libbrecht K.G. and Woodward M.F., 1990, Nature 345, 779
Libbrecht K.G., 1992, ApJ 387, 712
Morel P., Provost J., 1996, Priv. comm.
Palle P.L., Regulo C., and Roca Cortes T., 1989, A&A 224, 253
Palle P.L., Fossat E., Regulo C. et al., 1993, A&A 280, 324
Pantel A., 1996, Thesis, Université de Nice
Scherrer P.H., Wilcox J.M., Christensen-Dalsgaard J., 1983, Sol. Phys. 82, 75
Tomczyk, J. Schou, and M.J. Thompson, 1996, ApJ 488, L57
Toutain T., Appourchaux T., 1994, A&A 289, 649
Turck-Chièze S., Lopes I., 1993, ApJ 408, 347
Woodard M., 1984, Ph. D. Thesis, San Diego University

This article was processed by the author using Springer-Verlag LaTeX A&A style file *L-AA* version 3.